Excerpt from the Proceedings of the 2011 COMSOL Conference in Stuttgart

Optimization of the Gas Flow and Quality Check of a GEM Tracker

Valerie De Smet[*,1,3], Vincenzo Bellini[1,4], Evaristo Cisbani[2,5], Francesco Librizzi[4], Francesco Mammoliti[1,4], Michele Mangiameli[4], Francesco Noto[1,4], Concetta Maria Sutera[4].
[1]University of Catania - Italy, [2]Istituto Superiore di Sanità Roma - Italy, [3]Haute Ecole Paul-Henri Spaak ISIB, Brussels - Belgium, [4]INFN Sezione di Catania - Italy, [5]INFN, Sezione di Roma - Italy
*Corresponding author: Viale Santa Sofia 64, 95123, Catania, Italy, valerie.de.smet@hotmail.com

Abstract: In this paper we report results of a fluid-dynamics performance study of Gas Electron Multiplier (GEM) detector. The GEM technology has been proven to tolerate a rate larger than 50 MHz/cm^2 without noticeable aging and to provide the sub-millimeter resolution on working chambers up to 45x45 cm^2 [1]. A new GEM based tracker is under development for the upgrade of the Hall A equipment at Jefferson Lab. The chambers of the tracker have been designed in a modular way: each chamber consists of 3 adjacent GEM modules, with an active area of 40x50 cm^2 each [2]. We optimized the gas flow inside the GEM module volume, a mixture of Ar/CO_2 (70/30), using a COMSOL code. Our simulation includes design of the inlet-outlet pipes, maximization of the uniformity of the gas flux and minimization of the zones where such flux is too low.
Quality checks of GEM foil consist of: Optical and High voltage test. The first is an inspection of the anomalous sector(s) by using a microscope and the second is a high voltage test, in order to check leakage current in the GEM foil.

Keywords: GEM foil, Keitley6517B, Fluid Dynamics, Simulation

1. Introduction

In late 2014 the CEBAF electron beam at Jefferson Lab should complete the energy upgrade to 12 GeV. JLab will become one of the most important experimental facility for the study of the nucleon structure, in terms of form factors, transverse momentum distributions of the constituent partons and generalized parton distributions. New experimental equipment is under development for the optimal exploitation of the full potentiality of the new beam; a new hybrid tracker able to operate with luminosity as large as 10^{39} $s^{-1}cm^{-2}$ is part of this development. The tracker will provide an average single hit resolution better than 80 μm and an event readout frequency of about 30 kHz.

The tracker is made of two types of detectors: 40x50 cm^2 GEM modules and 10x20 cm^2 silicon μstrips. The former will be used as basic building blocks of large (~0.60 m^2) chambers that will seat behind a momentum analyzing spectrometer, while the latter will be positioned close to the scattering chamber, thus extending considerably the useful tracking arm. The hybrid design is aiming at a balance between cost and performances. The modular design of the GEM chambers (up to 6) intends to maximize reconfiguration on the existing or planned spectrometers of Hall A; each 40x50 cm^2 GEM module has its own readout, high voltage supply and gas inlet/outlet as well as front-end electronics. Mechanics and gas flow have been investigated and optimized by Finite Element Analysis. The single module is made of 3 GEM foils and a double layer x/y strip readout with 400 μm strip pitch. The modules are connected in a way to minimize the dead area and are supported by an external carbon fiber frame.

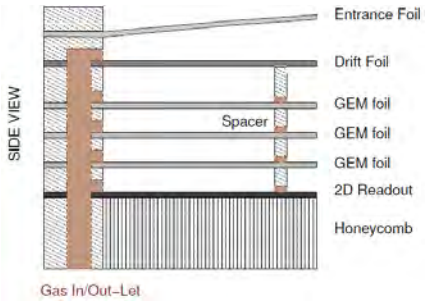

Figure 1: The triple GEM

2. Gas Input design

The role played by the gas mixture in the GEM detector is important. The avalanche process creates ions that pollute the gas what, diminishes the performance of the detector. Thus the gas has to be constantly replaced by new neutral one. The GEM structure being very thin, gas inlet and outlet pipes are limited in diameter. Hereafter we present a calculation of the minimal diameter of the pipe as function of the rate of renewing. The characteristic number that measures the ratio

between inertial and viscous forces is the Reynolds number:

$$Re := \frac{\rho V D}{\mu}$$

where ρ is the density (expressed in kg/m^3), V is the gas velocity (expressed in m/s), D is the diameter of the pipe (in m) and μ the dynamic velocity of the gas (in Pa/s). If we denote by $\Phi = \pi D^2 V/4$ the flux of the gas (expressed in m^3/s), we obtain, at fixed Reynolds number, then the diameter of the pipe is given by:

$$D = \frac{4}{\pi}\frac{\rho}{Re\,\mu}$$

To insure a laminar flow, the Reynolds number must not be greater than 2300. With a mixture of Ar/CO_2 (70/30), to insure a renewing of the gas of 10 times per hour, we find for the 10 cm x 10 cm test detector (using ρ = 1.7 kg/m^3 and $\mu = 2\times10^{-5}$ Pa/s and a thickness of 9 mm) we obtain a diameter of 3×10^{-4} mm.

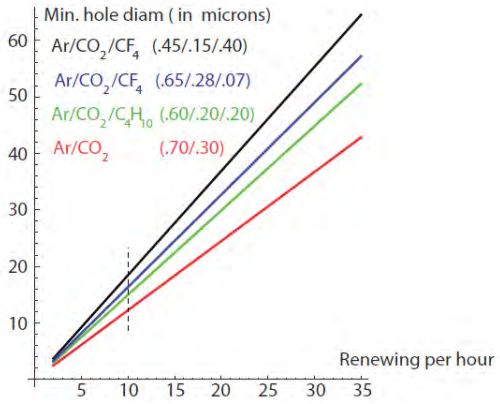

Figure 2: Minimal diameter of the input gas pipe, insuring a laminar flow, for different gas mixtures as a function of the rate of renewing of the detector enclosure gas.[10]

The diameter will varies linearly with the dimensions of the detector and with the rate of refreshing of the gas, and in inverse proportion to the viscosity of the gas. It will also depends on the temperature as the density decreases as T^{-1}, while in first approximation the dependence of the viscosity with respect to the temperature is given by the Sutherland empirical law:

$$\mu = \mu_0 \frac{T_0 + C}{T + C} (T/T_0)^{3/2}$$

Here C is the Sutherland's constant, that depends on the nature of the gas and is of the order of 200 (C_{Ar}=144; C_{CO2}=240). In a first approximation the diameter computed will depend as $(T_0/T)^{5/2}$ on the temperature, i.e. by a factor of the order of 0.9 between 15 °C and 25 °C . Another parameter that must be take into account is the dependence of the flux in the diameter of the pipe $\Phi \propto D^4$ in laminar regime, but this effect can be compensated by adjusting the pressure gradient. This dependence of the flux with respect to the diameter of the pipes justifies its optimization.

2. Simulation

The permanent gas flow in a module is required to provide the expected gain and signal timing, to evacuate gas that contaminates the mixture and to prevent fast aging of the detector due to radiation-induced chemical reactions in the gas. The gas flow should be spatially uniform in order to guarantee a homogeneous and stable detector response. Therefore, the goal of our study was to optimize the design of the frame separating two GEM foils in order to obtain a better gas flow uniformity over the active area of the module.

3. Use of COMSOL Multiphysics

The Finite Element Method approximates a Partial Differential Equations problem with a discretization of the original problem based on a mesh, which is a partition of the geometry into small units of simple shape called mesh elements. The PDE method looks for a solution in the form of a piecewise polynomial function, each mesh element defining the domain for one "piece" of it. Such a piecewise polynomial function will be expressed as a linear combination of a finite set of predefined basis functions. Let us consider for example a 2-dimensional problem with a single dependent variable p(x,y). We would like to solve this problem based on a mesh with quadratic triangular elements. The expression "quadratic elements" refers to the fact that on each mesh element the sought piecewise polynomial function $p^*(x,y)$ is at most a quadratic polynomial. In this case, the solution is expressed as:

$$p\,(x,y) \cong p^*(x) = \sum_{i=1}^{n} p_i \varphi_i(x,y)$$

where i refers to a node of the mesh, p_i are the degrees of freedom, $\varphi_i(x,y)$ are the basis functions and n is the total number of nodes, under the assumption that each triangle of the mesh possesses six nodes: three corner nodes and three mid-side nodes [4]. A basis function $\varphi_i(x,y)$ has here the restriction to be a polynomial of degree at most 2 such that its value is 1 at node i and 0 at all other nodes [5]. The degree of freedom p_i is thus the value of $p^*(x,y)$ at node i. The definition of the basis function associated to each node of the mesh can be derived using for example a general method introduced by Silvester in 1969 [6].

3.1 COMSOL's Thin-Film Flow Model

All of COMSOL's single-phase fluid flow interfaces are based on the three fluid dynamics conservation equations known as the Navier-Stokes equations [4], concerning the conservation principles of mass, momentum and energy:

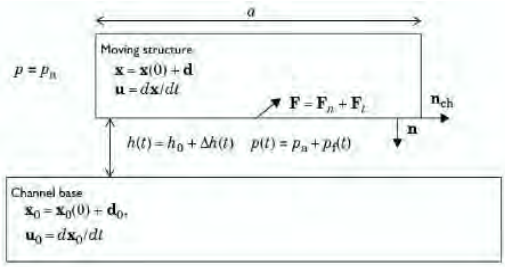

Figure 3: Schematic diagram of the situation to which the thin-Film Flow Model applies

The model that has been used in our simulations is the Thin-Film Flow Model [7] and belongs to the Computational Fluid Dynamics (CFD) module. The Thin-Film Flow Model model can be used to model a thin channel of fluid located between two moving structures, as schematized on Figure 2. The upper structure is referred to as the moving structure and the lower one as the channel base. Initially, both structures are surrounded by gas with a constant pressure pa and the fluid can freely move into and out of the gap. Due to the movements of the structures, an additional and usually time-dependent pressure p_f appears in the gas inside the gap, which produces a normal force $\overrightarrow{F_n}$ on the structures. Also a viscous drag force $\overrightarrow{F_t}$ is created which resists the tangential movement of the structure. In the Thin-Film Flow Model, it is however assumed that:

- The film thickness h remains always very small with respect to the dimensions of the solid structures.
- The channel curvature is small.

Also the following assumptions are made:

- The inertial effects in the fluid are negligible compared to the viscous effects, thus the flow is laminar.
- The pressure $p = p_a + p_f$ is constant over the film thickness h.
- The velocity profile over the film thickness is parabolic.
- The fluid is isothermal.

Given these assumptions, solving the fluid flow problem with the Navier-Stokes equations reduces to solving the following equation, called the Reynolds equation:

$$\frac{\partial(ph)}{\partial t} + \vec{\nabla}_{tg} \cdot (\rho h \vec{U}) - \rho(\vec{\nabla}_{tg}\, \Delta h_m \cdot u_m - \vec{\nabla}_{tg}\, \Delta h_b \cdot \overrightarrow{u_b})$$

where ρ is the density, $h = h_0 + \Delta h_m + \Delta h_b$ is the film thickness, t is the time, $\vec{\nabla}_{\mathrm{tg}}$ is a gradient computed only with the tangential derivatives along the channel boundaries, $\vec{U}$ is the mean film velocity, Δh_m and um are respectively the normal displacement and the tangential velocity of the so-called "moving structure", and Δh_b and u_b are respectively the normal displacement and the tangential velocity of the "channel base". The mean film velocity $\vec{U}$ is actually a function of the pressure p, the dynamic viscosity μ, the film thickness h, the tangential velocities u_m and u_b of the solid structures and the relative flow rate function Q_{ch} that accounts for possible rarefied gas effects:

$$\vec{U} = \frac{\vec{\nabla}_{tg}\, p}{12\mu} h^2 Q_{ch} + \frac{u_m + u_b}{2}$$

3.1.1. Simulations development

All the details on the selection of the physical parameters in the design of the GEM are taken from the ref. [3]

The geometry of the frame separating two GEM foils has been constructed in 2 dimensions, whereas the third dimension, which corresponds to the gas film thickness, has been inserted as a parameter of the physical model. Actually, two separate Thin-Film Flow models, have been defined in order to account for the two different

film thicknesses in the problem: 2 mm in between two GEM foils and 1 mm inside the openings of the frame's spacers and inside the inlets and the outlets.

As far as the inlets and outlets are concerned, it has not been possible to define their exact configuration, because this requires to use a physical model that can be applied to a geometry constructed in 3 dimensions. Therefore, we have defined inlets and outlets as 8x5 mm rectangular zones with a uniform film thickness of 1 mm.

Typical flows in gas detectors correspond to ⅓ volume renewals per hour. If the 3 GEM-modules of one chamber are connected to each other in series with respect to the gas flow, the total gas volume for a 2 mm thick "floor" of the chamber is approximately $3 \cdot 0.4 \cdot 0.5 \cdot 0.002 = 0.0012$ m^3, so ⅓ volume renewals per hour correspond in our case to gas flows between 20 cm^3/min and 60 cm^3/min. Nearly all our simulations have therefore been made with a total flow of 60 cm^3/min imposed at the inlets. In a frame with 2 inlets, having each a cross-section of 8 mm^2, the mean entrance velocity is then $U_e = 0.0625$ m/s. If one wants to evaluate whether such a stationary gas flow is incompressible or not, the mean velocity should be compared to the speed of sound in the same medium [4]. For an ideal gas, the speed of sound is given by the following formula:

$$U_s = \sqrt{\frac{\gamma RT}{M}}$$

where γ is the adiabatic constant of the gas, R = 8.314 J/(mol·K) is the universal gas constant, T is the temperature and M is the molecular mass of the gas. In our case, we consider that $\gamma \approx 5/3$ since argon is the main component of the gas mixture; T = 293 °K and $M \approx 0.70 \cdot 0.03995 + 0.30 \cdot 0.04401 = 0.04117$ kg/mol. For the speed of sound, we thus obtain $U_s \approx 314$ m/s >> $U_e = 0.0625$ m/s. Therefore, it has been assumed that the gas flow is incompressible and have used a constant value for the density ρ. Somehow, it's useful to get rid of the density's dependence on the pressure. The ambient pressure pa has been set to 1 atm. However, the solution for the velocity field does not depend on this value. The obtained velocity field does not depend either on the value of the constant density ρ which, for a Ar-CO_2 (70/30) mixture at 20 °C and 1 atm, can be computed using the densities at 20 °C and 1 atm of respectively argon and carbon dioxide ($\rho_{Ar} = 1.7837$ kg/m^3 and $\rho_{CO2} = 1.9770$ kg/m^3), with the following formula:

$$\rho = \left(0{,}30 \cdot \rho_{CO_2} + 0{,}70\rho_{Ar}\right) = 1{,}8417\,\frac{kg}{m^3}$$

To compute the dynamic viscosity at 20 °C and 1 atm of the gas mixture, we have used Reichenberg's formula [9] with the parameters from the literature and we have obtained:

$$\mu = 1.9696 \cdot 10^{-5} \text{ Pa·s.}$$

In the two defined Thin-Film Flow Models, instead of considering two moving solid structures, we have forced the normal displacements, Δh_m and Δh_b, and the tangential velocities, u_m and u_b, of these structures to zero, so that the film thickness h would remain constant to its initial value h_0. We have also assumed in the first place that the fluid can be treated as a continuum. Actually, the Knudsen number obtained with our no-slip models was around $5 \cdot 10^{-5}$, which is indeed negligible with respect to 0.1.In our case, the ambient pressure p_a has been set to 1 atm, and as boundary conditions:

- We have imposed a uniform perpendicular velocity (e.g. 0.0625 m/s) on the external 8 mm side of the inlets.
- On the external 8 mm side of the outlets, we have forced the additional pressure p_f to zero.
- "Walls" have been inserted on the sectors of the geometry that represent surfaces of the frame. This imposes the standard wall boundary condition $\vec{U} = \vec{0}$ on these sectors.

When simulating a system that is quite complex, it's advised to start with a strongly simplified geometry and increase progressively the complexity of the model, as one's knowledge of the simulation increases [4]. We have started by simulating a frame with only two sectors, separated by a spacer containing just one opening of length 15 mm. One inlet (with velocity 0.0625m/s) and one outlet have been defined. The problem has been treated as stationary and a predefined mesh type of COMSOL ("Normal") has been used, which in our case is made up of 24182 unstructured quadratic triangular elements. The obtained velocity field is shown in Figure 4.

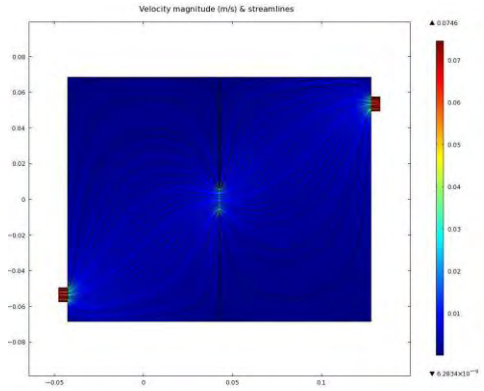

Figure 4: Velocity magnitude on a linear scale and streamlines of the velocity field obtained in the case of a frame with 2 sectors 1 inlet at the left and 1 outlet at the right. The two sectors communicate throught a central opening of 15 mm.

In a next step, we have simulated six adjacent sectors of the frame and included two 15 mm openings in each spacer. It has been useful to define a time-dependent model in which the inlet velocity increases smoothly from 0 to 0.0625 m/s. We are however not mainly interested in this evolution and we focus on the results obtained for the final state (Figure 5). In this simulation, we have also tried out a more complex mesh, consisting of a predefined "Fine" unstructured quadratic triangular mesh in the central regions (133276 elements) and a "Boundary Layer", made up of parallel rectangular quadratic elements along the borders of the geometry (39252 elements). Notice that on Figure 5, the scale has been cut at a tenth of the maximum velocity.

Based on these results, we have tried to modify some aspects of the frame's design in order to reduce, in number and/or in size, the zones with particularly high or low velocities. The optimization of the frame design has been realized by gradually modifying the simulated geometry and comparing each time the new results with those from previous simulations.

In all our simulations of full-sized frame versions, we have used the time-dependent model but without working with the same type of mesh as in the six-sectors simulation, because of the too large number of elements (over 500000). We have defined another type of customized mesh consisting of three predefined unstructured quadratic triangular mesh types:

- in the inlets and outlets, as well as in a 16 x 10 mm^2 rectangular zone in front of each of them, we have defined a "Finer" (resp. "Extremely fine") mesh, in the first two simulations (resp. the last four ones).
- in a 15 mm (resp. 20 mm) thick zone along all the other boundaries, we have defined a "Fine" (resp. "Extra fine") mesh, in the first two simulations (resp. the last four ones).
- in the rectangles left over in the center of the several frame sectors, we have defined a "Normal" (resp. "Finer") mesh, in the first two simulations (resp. the last four ones).

In this way, we have tried to refine our meshes without exceeding 250000 elements. Since the geometry is different in every simulation. In order to assess in some way the precision of our various simulations, we have compared for each simulation the inlet and the outlet total fluxes based on the computed velocity field. Since the flow is supposed to be conserved, these fluxes should in theory be equal and, of course, correspond to the initially imposed value (e.g. 60 cm^3/min).

3.1.2 Analysis and results

3.1.2.1 Simulation 1: Full frame in its first prototype version

In its first prototype version, the frame separating two GEM foils possesses 18 sectors, 2 inlets and 2 outlets. Two adjacent sectors along the longest side of the module communicate through 2 openings of 15 mm, while two adjacent sectors along the other direction communicate through a single 15 mm opening. In our simulation, the uniform velocity imposed on both inlets is 0.0625 m/s, which corresponds to a total flow of 60 cm3/min. Notice that the scale has been cut at a tenth of the maximum velocity. A contour plot with logarithmic scale of the velocity magnitude is also given in Figure 6.

As expected, the zones with lower velocities are found mainly in corners where spacers cross each other or reach the border of the frame, and in the four corners of the outer structure of the frame. However, our attention has also been drawn towards two large low flux zones at the extremities of the central 6-sectors row, which contains no inlets and outlets. For this reason, in

our next simulation we have included an extra inlet and outlet, placed at the level of this central row.

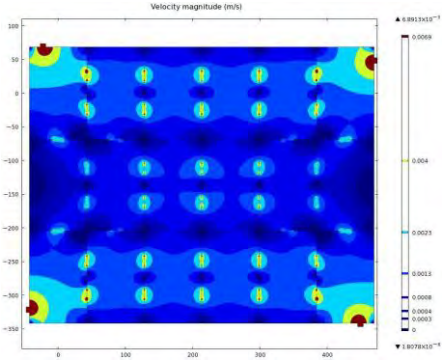

Figure 6: Simul. 1 – Contour plot with logarithmic scale of the velocity magnitude obtained in the case of the full frame in its first prototype version.

Zones with higher velocities correspond to inlets, outlets and openings in the spacers, especially in the spacers parallel to the shortest side of the module. Figure 7 shows a close-up on one of the inlets. Although our simulation isn't the most appropriate to estimate the actual velocity field in the region of inlets and outlets, we can realize from it that the 90° angles between an inlet (or outlet) and the borders of sectors are responsible for particularly high velocities, which are in fact also much higher than in the openings of spacers (Figure 9). The maximum velocity computed by the simuation (0.0689 m/s) is indeed found on these edges at the inlets and outlets. Thereupon, we have decided also to replace in our next simulation these 90 degrees edges by circular joints of radius 1.5 mm.

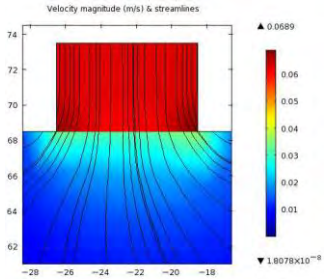

Figure 7: Simul. 1 – Velocity magnitude on a linear scale and streamlines of the velocity field obtained for one of the two inlets in the first prototype version.

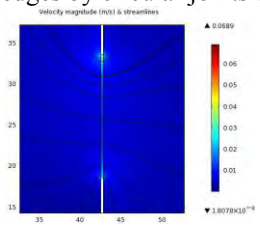

Figure 8: Simul. 1 – Velocity magnitude on a linear scale and streamlines of the velocity field obtained for an opening in a spacer of the full frame in its first prototype version.

3.1.2.2 Simulation 2: Modifications to the inlet and outlet configuration

In this second simulation, one inlet and one outlet have been added with the aim to improve the uniformity of the gas flow in the central 6-sectors row of the frame. The exact positions of these inlet and outlet have been selected based on the available space in the detector. For all inlets and outlets, the aforementioned circular joints of radius 1.5 mm have also been introduced. The 60 cm^3/min flow has been maintained, resulting in an inlet velocity of 0.04167 m/s. In Figure 9, the obtained velocity magnitude is shown on a linear scale (cut to a tenth of the maximum velocity), together with the streamlines. Figure 11 is a contour plot of the velocity magnitude with a logarithmic scale.

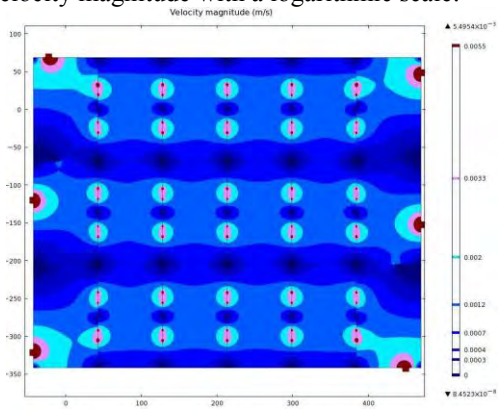

Figure 9: Simul. 2 – Contour plot with logarithmic scale of the velocity magnitude obtained for an 18 sectors frame with 3 inlets (left) and 3 outlets (right).

On a qualitative basis, the overall uniformity of the velocity magnitudes looks improved by the added inlet and outlet. It seems that in this configuration we obtain in the six-sectors rows three relatively independent and similar flows. In order to show the effect of the circular joints at inlets and outlets (cf. Figure 11), we have also run the same simulation using the initial geometry of the inlets and outlets. Figures 10 and 11 share the same color scale, so that the slight reduction of the high velocities inside the sector is visible for the design with circular joints. It will help avoiding their separation from the walls and thus avoiding possible small turbulence areas near the inlets and outlets.

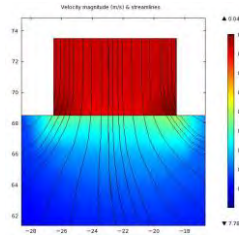

Figure 10: Simul. 2 bis – Inlet without circular joints

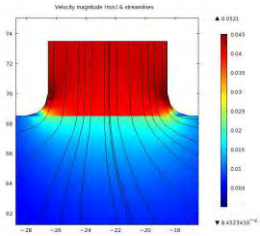

Figure 11: Simul. 2 – Inlet with 1.5 mm radius circular joints

3.1.2.3 Simulation 3: Reduction of the number of sectors from 18 to 12

Since low velocity zones are found where spacers cross each other or reach the border of the frame, reducing for example the number of spacers would be a way to reduce these "stagnation" zones in number, which might thus improve the overall uniformity of the gas flow. A sector of a GEM-foil glued to its frame can be modeled as a built-in rectangular thin plate of area S, being stretched by a uniform force per unit length T at its circumference, and undergoing a normal pressure P. The maximum deformation u_{max} of such a plate is given by the following expression:

$$u_{max} = k\,(\zeta) = \frac{PS}{T}$$

where the geometrical factor κ(ζ) is an increasing function of the ratio ζ ∈]0, 1] of the rectangle sides. For a square plate, κ reaches a maximum value of nearly 0.074. In our case, we want the maximum deformation u_{max} to remain lower than 1% of the 2 mm thick gap between two GEM foils, at a pressure P up to 10 N/m^2, when a tension of 1 kg/cm (T = 9.81 N/cm) is applied to the GEM foil. If we consider in first approximation a geometrical factor κ of 0.074, the maximum allowable area S of a sector should thus be:

$$S = \frac{u_{max}T}{kP} = \frac{2 \cdot 10^{-5} \cdot 9.81 \cdot 10^{2}}{0.074 \cdot 10} = 2.65 \cdot 10^{-2} m^2$$

Based on these assumptions, it would have been feasible to reduce the number of sectors to only 9 (using 2 spacers along both directions), since the area of each sector would have been equal to $\frac{0.2}{9}\ m^2 = 2.22 \cdot 10^{-2}\ m^2$. However, a more conservative choice of 12 sectors (2 spacers along the long side and 3 spacers along the short one) has been made, which results in sectors of about 0.125 x 0.133 m^2 = 1.66 · 10^{-2} m^2. The Figures 14 and 15, showing the simulation results for a frame with 12 sectors, the overall uniformity of the gas flow seems indeed improved by the reduction of the number of spacers along the shortest side of the module.

3.1.2.4 Simulation 4: Enlargement of some openings in the spacers

With the hope to further improve the flow uniformity, especially in the sectors possessing an inlet or an outlet, we have made a simulation in which the openings in the spacers that delimit these particular sectors are enlarged from 15 to 20 mm. The results have however not been so convincing. For this reason, the idea of modifying the width of the openings in spacers has been abandoned.

.

3.1.2.5 Simulation 5: Nine openings in the spacers along the short side of the module

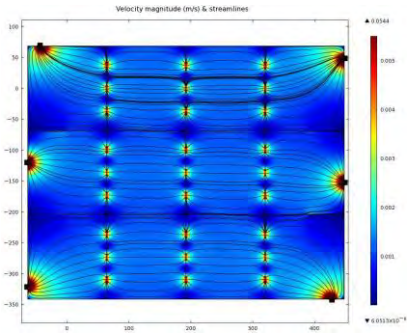

Figure 12: Simulation 5 – Velocity magnitude on a linear scale and streamlines of the velocity field obtained for a 12-sectors frame with 3 inlets (left) and 3 outlets (right), having nine 10 mm openings in the spacers along the short side of the module.

Good results have been obtained with nine openings of 10 mm instead of six openings of 15 mm for the spacers along the short side of the module. When comparing Figure 12, with the figures from previous simulations, we notice a reduction in size of the low velocity zones where spacers cross each other and where the short spacers reach the longest border of the frame.

3.1.2.6 Simulation 6: Doubling the openings in the spacers along the long side of the module

After the results of Simulation 5, we have tried to find out whether doubling the number of 15

mm openings in the spacers along the longest side would decrease the size of the large low velocity zones near the shortest borders of the frame. However, these long spacers are parallel to the main direction of the gas flow, instead of

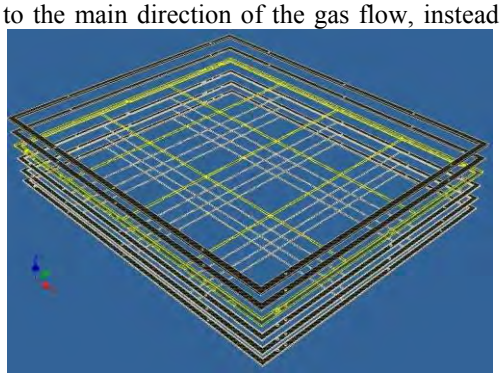

Figure 13: All frames of the module assembled

being perpendicular to it like the short spacers. For this reason, increasing the number of openings in the long spacers does not produce the same positive effect on the flow uniformity. We have decided in consequence to stick with the frame design of Simulation 5, since in Simulation 6 we have not found a sufficient improvement of the flow uniformity to justify adding openings in the long spacers and thus weakening the mechanical support they provide. The new frame designs are shown in figure 13.

4. Quality checks of GEM foils

Resistivity on air between the two sides exceeds 2 GΩ per sector and the hole diameter and pitch are 70±5 μm and 140±5 μm respectively, the GEM foils can be delivered. Only GEM foils which pass optical inspection and high voltage test, can be used to build a GEM module. Quality checks of GEM foils are important, because impurities, scratches, etching defects, such as missing holes, joint holes, overhanging copper and cracks in the Kapton, will affect the amplification properties of a foil.
In particularly, the quality checks of GEM foils consist of:

- Optical inspection
- High voltage test

4.1 Optical inspection

A manual optical inspection of GEM foil is done in order to assess its global state (mainly the cleanness and the presence of scratches). Then, GEM foil undergoes high voltage test. If GEM foil doesn't show expected behavior during the high voltage test, a more extensive optical inspection of the anomalous sector(s) is performed manually by microscope in order to localize cause of the problem.

4.2 High voltage test

GEM foil should be placed inside a clean Plexiglas box that is flushed with dry nitrogen gas in order to reduce the moisture level and provide a stable and reproducible environment. Before applying voltage, flushing closed box during 2 or 3 hours is necessary to evacuate air and contaminating impurities. The aim of high voltage test is to check leakage current through insulating Kapton GEM foil's layer when a voltage is applied on the two external copper layers.

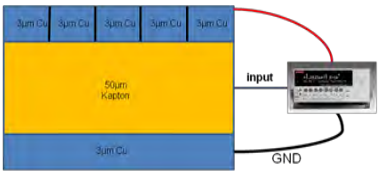

Figure 14: Schematic view of the voltage applied on the two external copper layers with Keithley 6517B

An anomalous behavior during the test could indicate the presence of defects in the foil, so in this respect the high voltage test plays a crucial role in the quality control of GEM foils. During the test, the voltage should be increased progressively, by "steps", because strong discharges should be avoided. Test can be performed sector by sector or on the whole GEM foil. In Catania, the high voltage tests of GEM foils will be performed by using an electrometer Keithley 6517B, which will apply voltage and measure the leakage current. This device has a voltage source that can deliver up to 1000 V and currents can be measured between $1 \cdot 10^{-18}$ A and 20 mA (10 current ranges available). For current measurements, an internal connection should be configured, by using the "meter-connect" option.

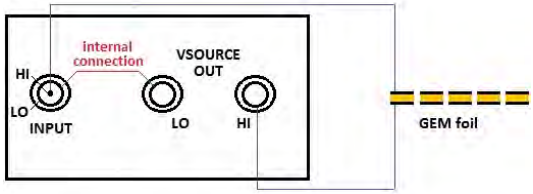

Figure 15: Schematic view of the connections between the electrometer Keithley 6517B and GEM foil.

For the remote control of Keithley 6517B in the high voltage test of GEM foils, a LabVIEW program has been developed. The advantages of the remote control are that the voltage ramps are automatically generated, the current measurements are automatically performed, the measured values can be systematically recorded in a text file and the evolution of the test can be followed on a graphic that displays the measured current in real time.
Keithley uses the LABVIEW program which communicates with the pc by the RS232 protocol.
The quality test performed by JLAB12 group of Catania regarded a 40 x 50 cm GEM foil. First the void resistance of GEM foil was measured. It was performed in all sectors (typical value is upper 1GOhms): in other sectors, resistance value was about 4 KOhm. Sectors with low resistance were analyzed by a microscope. The anomalies were mapped for all sectors and have been cleaned in front and back side of GEM foil, but many scratches and impurities cannot be eliminated.
By applying a voltage of 100V, I is about 54nA. The test was stopped and resistance of the sectors of interest was measured to be about 4 KΩ (2 sectors were isolated and excluded from the test). Successively a voltage was applied to the remaining sectors: for V=100V, I=3nA and for V=250V, I=50nA. At this stage, by applying the tension to the remaining sectors, the limit tension was calculated for the single sectors. For example the figure 17 shows the V-I characteristics of sector 4.

Figure 16: Schematic representation of the gem foil tested with the sectors numeration. In red the sectors isolated with Kapton

Differences among limit voltages are due to the impurities and construction anomalies which characterize each sector.

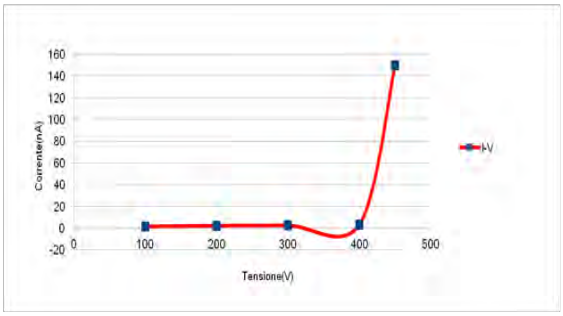

Figure 17: V-I characteristics of sector 4 (for example)

5. Conclusion

Our goal has been to obtain a better spatial uniformity (over the active area of the module) of the continuous Ar-CO_2 (70/30) gas flow in the 2 mm gap between two GEM foils, since this gas flow should be spatially uniform in order to guarantee a homogeneous and stable detector response. With a frame geometry defined in two dimensions, we have used the built-in Thin-Film Flow Model, which treats the laminar and isothermal flow of a thin fluid film between two large solid structures and solves the corresponding Reynolds equation. We have defined a typical total gas flow of about 3 chamber-volume renewals per hour (60 cm^3/min) and this gas flow has been considered incompressible. The optimization of the frame design has been presented through mainly six simulations, showing progressive modifications of the simulated geometry. The initially defined geometry corresponds to the first prototype version of the frame, possessing eighteen sectors, two inlets and two outlets. A second simulation has shown that adding a third inlet and a third outlet improves the overall flow uniformity, as the flows in the three six-sector rows become rather independent and similar. High velocity zones nearby inlets and outlets have also been reduced by replacing 90 degrees edges with 1.5 mm radius circular joints. In a third simulation, the number of stagnation zones has been decreased by reducing the number of short spacers from five to three, leading to a frame with twelve sectors which still meets the mechanical requirements related to the planarity

of the GEM foils. The fourth simulation, in which openings in the spacers nearby the inlets and outlets have been enlarged from 15 mm to 20 mm, has not yielded a meaningful improvement of the gas flow uniformity. However, the fifth simulation has shown that introducing in the short spacers nine openings of 10 mm, instead of six openings of 15 mm, decreases the size of various stagnation zones. Finally, we have concluded from a sixth simulation that doubling the number of 15 mm openings in the long spacers does not significantly improve the flow uniformity and thus the geometry of the fifth simulation has been selected as the basis for a new frame design.

The quality control has enabled us to analyze the detector by visually inspecting the impurities that affect the operation and determining the the maximum stresses applied to the fields.

In particular for low voltage, the sectors 1, 2, 3 broke.

6. References

[1] M. Alfonsi et al " Activity of CERN and LNF groups on large area GEM detectors" Nucl. Instr. Meth. A 617 (2010) 151.

[2] J. Alcorn et al - "Basic instrumentation for Hall A at Jefferson Lab", Nucl. Instr. Meth. A 522 (2004) 294.

[3] Valerie De Smet, Study of a GEM tracker of charged particles for the Hall A high luminosity spectrometers at Jefferson Lab, Master thesis, 2011

[4] Felippa C.A., Introduction to Finite Element Methods, lecture notes, Department of aerospace engineering sciences of the University of Colorado, Boulder, 2004.

[5] COMSOL Multiphysics User's Guide v4.1, COMSOL A B, 2010.

[6] Lewis R.W., Nithiarasu P. & Seetharamu K.N., Fundamentals of the Finite Element Method for Heat and Fluid Flow, New York, John Wiley & Sons, 2004.

[7] CFD Module User's Guide v4.1, COMSOL AB, 2010.

[8] Alfonsi M. et al., Aging measurements on triple-GEM detectors operated with CF4-based gas mixtures, Proceedings of the 9th Topical Seminar on Innovative Particle and Radiation Detectors, Nuclear Physics B – Proceedings Supplements, Volume 150, pages 159-163, BIBLIOGRAPHY 119 January 2006.

[9] Poling B.E., Prausnitz J.M. & O'Connell, The properties of gases and liquids, 5th edition, New York, McGraw-Hill, 2004.

[10] Spindel P., Contribution to the set up of a Gas Electron Multiplier detector, Master thesis, Catania, 2009.